IOP Publishing Reports on Progress in Physics
Rep. Prog. Phys. **82** (2019) 012001 (18pp) https://doi.org/10.1088/1361-6633/aad3e5

Key Issues Review

Manipulating the flow of light using Dirac-cone zero-index metamaterials

Daryl I Vulis, Orad Reshef, Philip Camayd-Muñoz and Eric Mazur[1]

Department of Physics and School of Engineering and Applied Sciences, Harvard University, 9 Oxford Street, Cambridge, MA 02138, United States of America

E-mail: mazur@harvard.edu

Received 11 January 2016, revised 5 April 2018
Accepted for publication 17 July 2018
Published 5 November 2018

Corresponding Editor Professor Masud Mansuripur

Abstract

Metamaterials with a refractive index of zero exhibit properties that are important for integrated optics. Possessing an infinite effective wavelength and zero spatial phase change, zero-index metamaterials may be especially useful for routing on-chip photonic processes and reducing the footprint of nonlinear interactions. Zero-index has only been achieved recently in an integrated platform through a Dirac-cone dispersion, enabling some of these more exciting applications in an integrated platform. This paper presents an overview of Dirac-cone zero-index metamaterials, including the fundamental physics, history and demonstration in the optical regime, as well as current challenges and future directions.

Keywords: metamaterials, zero-index, nanophotonics, Dirac-cone

(Some figures may appear in colour only in the online journal)

Contents

1. Introduction 1
2. Zero-index properties 2
   2.1. Wavelength and phase 3
   2.2. Optical wave impedance 3
   2.3. Dispersion and causality 4
3. Design and demonstration of Dirac-cone ZIM 5
   3.1. Tuning permeability 5
   3.2. Mie theory and effective medium properties 7
   3.3. Theoretical prediction and first appearances 8
   3.4. Optical ZIM 8
4. Challenges of Dirac-cone ZIM 10
   4.1. Tolerance to fabrication imperfections and tunability 10
   4.2. Device height 11
   4.3. Modal degeneracy and band structure 12
   4.4. Treatment as a homogeneous material 13
   4.5. Losses 15
5. Outlook 15
Acknowledgments 16
References 16

[1] Author to whom any correspondence should be addressed.

1. Introduction

Recent decades have seen significant advances in integrated optics. Once considered to be the solution to the limits of electronics [1, 2], the emergent field of nanophotonics has instead enabled access to entirely new and unanticipated physical regimes. In reaching the nanoscale, light can experience longer interaction lengths and smaller effective mode areas. However, the dimensions of these integrated nanophotonic devices have an inherent dependence on operating wavelength, in stark contract to the design freedom associated with the static fields of electronics. Beating the diffraction limit, or otherwise decoupling wavelength and device size, has remained a fundamental challenge in the field. Materials with specifically tailored properties could provide a different avenue to circumvent the diffraction limit. Metamaterials—composite

materials engineered through the structuring of subwavelength constituents—have emerged as a method of achieving unnatural properties, among them a negative or zero refractive index.

There has been significant recent interest in materials with a refractive index of zero [3–5]. A notable property of zero-index materials is an infinite effective wavelength. The 'stretched' wavelength within a zero-index material can be exploited to entirely decouple the relation of material footprint to performance, allowing for extreme flexibility in the design of single-mode resonators [4, 6, 7]. In essence, as the wavelength extends far beyond to the boundaries of a zero-index material, the exact footprint of the device becomes irrelevant. This unique property has inspired a variety of applications including efficient coupling between disparate modes [8–10], electromagnetic cloaking [11, 12], relaxed phase matching constraints [13] and enhancement in nonlinear optics [14–16].

Zero-index phenomena are uncommon in natural materials. However, the definition of the refractive index,

$$n = \sqrt{\mu\epsilon}, \tag{1}$$

reveals that the index of a material is determined by its response to both the electric and magnetic fields of light as quantified by the permittivity (ϵ) and permeability (μ). A zero-index is achieved when one or both of these parameters equal zero, knowledge that has recently led to numerous experimental zero-index demonstrations for which only the permittivity is equal to zero (commonly referred to as ENZ materials). Metals achieve ENZ conditions at the ultraviolet plasma frequency, an example of naturally occurring zero-index behavior [17]. A similar effect is observed in parallel plate waveguides operating at their cutoff frequency [18], which have been used to demonstrate ENZ phenomena at visible frequencies [19]. ENZ materials have since been realized at optical frequencies for continuous media such as transparent conducting oxides (TCOs) [20–22], as well as metamaterials with metallic inclusions [23–26].

A significant limitation of ENZ materials is the high reflectivity that results from an infinite impedance defined as [27, 28],

$$\eta = \sqrt{\frac{\mu}{\epsilon}}. \tag{2}$$

Furthermore, these materials are incapable of transporting energy due to a vanishing group velocity [29]. These limitations are eliminated if the magnetic permeability is also equal to zero, producing a finite impedance and non-zero group velocity. To this end, the past few years have seen the advent of all-dielectric Dirac-cone zero-index metamaterials (ZIMs). These metamaterials consist of dielectric resonators with magnetic and electric responses that can be tuned to simultaneously cross zero for a given frequency. Coincident magnetic and electric resonances produces a modal degeneracy in the photonic band structure which appears as the intersection of two linear bands at the Γ-point, or a Dirac-like cone [30–34]. This dispersion profile is analogous to the electronic dispersion of graphene, which features a similar linear band crossing at the *K*-point of a hexagonal lattice [35]. Dirac-cone ZIMs not only eliminate the intrinsic losses associated with metals, but also possess finite impedance that enables compatibility with integrated photonics.

Dirac-cone metamaterials offer a refractive index of zero for operation in the optical regime that can be achieved using standard CMOS processing [34, 36, 37]. Especially important for integrated applications, these metamaterials are accessible from an in-plane orientation that matches the optical excitation produced by planar waveguides. The ZIMs consist of a 2D unit cell array that can be based in several common high-index dielectrics, notably the material that has dominated integrated photonics in recent years, silicon. The choice of material and tuning of resonator geometry allows for unprecedented flexibility in the selection of operation frequency. Furthermore, these metamaterials can be fabricated in variable shapes through the reconfiguration of the constituent resonator-based unit cells. Such ZIMs enable access to the aforementioned exotic phenomena through an integrated platform that is compatible with both standard planar fabrication methods and the existing library of integrated electronic and photonic devices.

In addition to a refractive index of zero, implementation of a Dirac-cone dispersion offers further advantages. These platforms provide easy access to directly study Dirac physics and its related topological properties [38]. Furthermore, they have been used to generate and control exceptional points [39, 40], for light trapping [41] and arbitrary control of electromagnetic flux [11, 42, 43]. Dirac-cone ZIMs have been proposed for varied applications, such as large-area single-mode lasing [6, 7], beam steering (or leaky-wave antenna) [44, 45], and lensing [46]. Additionally, photonic Dirac cones have also been shown to provide enhancements to the nonlinear optical response [47–49], and to optical cross-sections [39].

Dirac-cone ZIMs possess properties that are promising for integrated optics applications (explored further in *zero-index properties*). Recent demonstrations have ranged from microwave to optical frequencies and showcased significant advances towards developing an accessible platform (explored further in *design and demonstration of Dirac-cone ZIM*). However, they have not reached an iteration suitable for wide-spread implementation. Challenges include unreliable fabrication, significant radiative losses, and differences in behavior as compared to bulk zero-index materials (explored further in *challenges of Dirac-cone ZIM*). However, we emphasize that these issues are not always inherent to the zero refractive index or Dirac-cone ZIMs. This review will explore some of the obstacles and solutions that can be addressed to make Dirac-cone ZIMs reach their full potential in revolutionizing integrated optics.

2. Zero-index properties

Dirac-cone ZIMs enable access to exotic zero-index phenomena. The wavelength in a ZIM is elongated to the boundaries of the material and a phase advance of zero is observed throughout. However, the zero-index must be achieved via simultaneously zero permittivity and permeability values to enable finite impedance. Finally, a refractive index of zero results in unexpected dispersion and causality relations with

respect to band structure, pulse propagation, impedance, and group velocity. The following section explores the behavior and physical implication of these properties with emphasis on the effects of a Dirac-cone implementation.

2.1. Wavelength and phase

A refractive index of zero enables access to extreme physical phenomena that can be predicted directly from the wave equation. The refractive index dictates the propagation of light within a material, particularly the rate of phase accumulation that defines the wavelength. As propagating waves transition between materials of different indicies, the wavelength changes in proportion to the index. Light entering a material with a larger refractive index propagates with a shortened wavelength, whereas wavelength of light entering a smaller refractive index material is lengthened. If a wave enters a material with vanishing refractive index, the wavelength extends to infinity (figure 1). At this limit, the fields are uniform throughout the zero-index material, and no phase is accumulated.

Optical propagation is fully described by the electromagnetic wave equation,

$$\nabla^2 E - \frac{\mu\epsilon}{c^2}\frac{\partial^2 E}{\partial t^2} = 0. \tag{3}$$

As equation (3) shows, the optical response within a given material can be fully characterized by two quantities—the electric permittivity (ϵ), and its counterpart, the magnetic permeability (μ). Consequently, the refractive index as defined in equation (1), dictates the form of solution to equation (3).

When the refractive index is equal to zero, the spatial and temporal terms of equation (3) are decoupled and the resulting spatial component ($\nabla^2 E = 0$) reveals out-of-plane electric fields (corresponding to E_z) that oscillate in time, but not space [12, 43]. A field that oscillates only in time has a wavelength that is 'stretched' beyond the boundaries of the material, effectively infinite (figure 1). A further consequence is a field distribution that is entirely uniform, oscillating in unison. This 'phase-free' profile can be considered analogous to the behavior of static fields in electronics, allowing for light in a zero-index material to experience an effectively infinite phase velocity (v_p) regardless of footprint. This decoupling firmly establishes the distinction of zero-index physics from limitations long associated with integrated optics: static field effects can be accessed at optical frequencies, producing an optical material that may behave as an electric conductor with implications of significantly improved on-chip routing and control.

2.2. Optical wave impedance

The expected static field effects have been commonly achieved in zero-index materials for which only the permittivity is equal to zero [4, 20–25]. Commonly referred to as ENZ materials, the impedance of these materials is a significant obstacle for integrated applications. ENZ materials (and their magnetic counterparts with a permeability of zero, MNZ) possess a divergent impedance as described by equation (2), leading to strong reflections. In the case of ENZ (MNZ), power reflection defined as,

$$R = \left(\frac{\eta_{\text{in}} - \eta_z}{\eta_{\text{in}} + \eta_z}\right)^2, \tag{4}$$

is unity in cases of $\eta_{\text{in}} = \infty$ ($\eta_{\text{in}} = 0$), indicating total reflection at the boundary of ENZ (MNZ) materials when excited from any adjacent medium [26].

However, this impedance mismatch can be overcome by engineering the footprint of an ENZ waveguide. Using transmission line analysis, ENZ materials within a parallel plate waveguide can achieve finite impedance through purposeful arrangement of the boundaries [50]. These ENZ materials obey a modified expression for wave impedance,

$$\eta_i = a_i/b_i\sqrt{\frac{\mu_i}{\epsilon_i}}, \tag{5}$$

where the subscript i denotes the section of waveguide, a refers to the width of the channel, and b refers to the height of the channel. From this point on, b_{i} is assumed to be uniform and is omitted in the equations. (figure 2). In the case of an ENZ coupler joining two waveguides, complete transmission is achieved when all three components are impedance matched. If the input and output channels are identical, impedance matching is achieved for

$$\frac{a_{\text{in}}}{a_z} = \sqrt{\frac{\mu_z}{\epsilon_z}}. \tag{6}$$

In the case of ENZ couplers, transmission is maximized for subwavelength dimensions. Complete transmission has been verified theoretically for ENZ 'super'-couplers [8, 9, 50] and experimentally at both microwave [51, 52] and optical frequencies [19]. Conversely, MNZ couplers experience maximum transmission for heights that significantly exceed the waveguide dimensions; the behavior of MNZ couplers has been verified theoretically and experimentally [53, 54].

However, for zero-index materials resulting from both ϵ and μ near zero (EMNZ), the relation between waveguide dimension and impedance is decoupled [10, 43, 55]. The result is complete flexibility in the dimensions of the zero-index coupler, highlighting a unique feature of EMNZ materials as compared to ENZ or MNZ materials. These relations generally hold for both bulk zero-index materials and metamaterial ZIMs, however, the latter necessitates additional considerations. Any bulk ENZ, MNZ, or EMNZ waveguide supports a single, zero-index mode. However, Dirac-cone ZIMs intrinsically support an additional mode at the zero-index frequency that can convolute the transmission line model. Generally, access to this mode can be avoided entirely through operation at a slightly higher frequency [30, 33, 34] (See *Homogenization*), resulting in a slightly positive index while retaining much of the high transmission capabilities.

Furthermore, ENZ and MNZ cases can occur in Dirac-cone ZIMs but generally result in a non-transmitting photonic bandgap (See *Dispersion*). As most unit cells are not significantly subwavelength, it is difficult to achieve the dimensions necessary for high transmission in ENZ operation. This could,

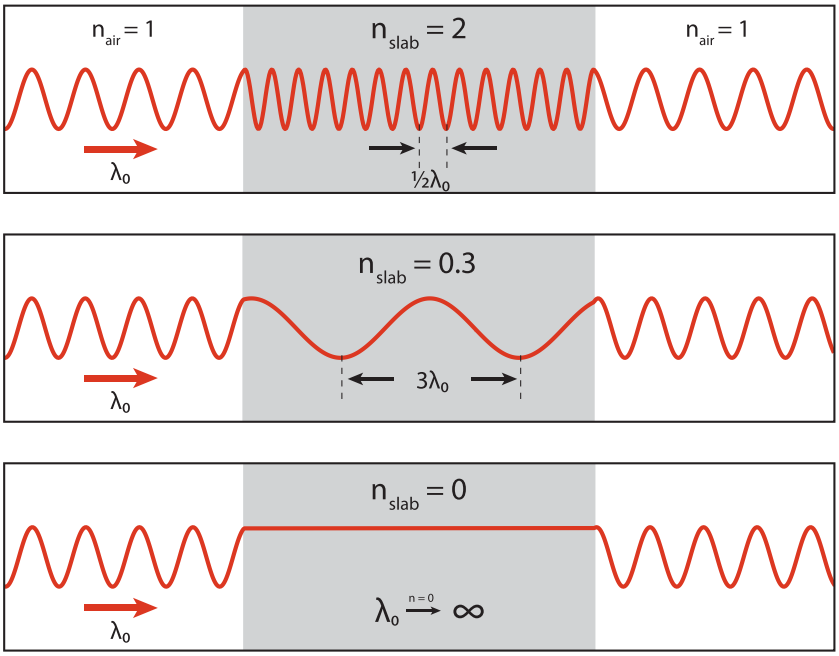

Figure 1. The wavelength of light propagating through dielectric media is changed in inverse proportion to the refractive index. The wavelength extends to infinity as the real portion of the refractive index decreases to zero.

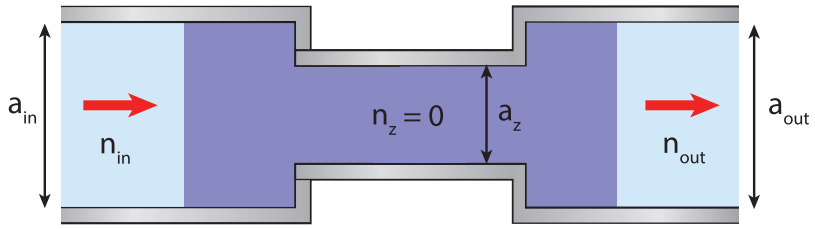

Figure 2. Schematic of a zero-index waveguide coupler; *a* denotes the waveguide dimensions, *b*, which denotes the height of the coupler, is assumed to be uniform and omitted. *n* denotes the refractive index.

however, be circumvented in future work by developing unit cells that possess dimensions smaller in relation to the operating wavelength.

2.3. Dispersion and causality

Effective operation of a zero-index material in an integrated capacity has additional requirements beyond the strong transmission of a plane wave source. The typical unit of information transfer, an optical pulse, involves the superposition of a spectrum of frequencies, highlighting the importance of dispersion. Notably, the linear dispersion relation, an intrinsic property of Dirac-cone ZIMs, corresponds to zero group velocity dispersion ($\frac{\partial^2 k}{\partial \omega^2}$) which is necessary to avoid distortion of an optical pulse. This quantity is directly linked to wave impedance as the latter results from the ratio between the dispersion of the permittivity and the permeability when both values are close to zero. These dispersions are a direct consequence of the unit cell properties (i.e. resonator dimensions, arrangement, and material) and cannot be altered without an additional degree of freedom (see *Tolerance to fabrication imperfections and tunability*).

The infinite phase velocity resulting from coordinated field oscillation in zero-index materials has raised the question of whether zero-index materials violate causality by featuring 'superluminal' propagation. Such a propagation scheme would enable instantaneous transfer of an optical pulse at a phase velocity that exceeds that of light in a vacuum, *c*. However, to permit the transmission of an optical pulse at superluminal speeds, a refractive index of zero would need to be achieved for the entire bandwidth of the pulse, yielding a *group* velocity larger than *c* [56–59]. This is not possible without strong dispersive absorption or gain. In contrast, causal Dirac-cone ZIMs possess a linear dispersion for which causality can be verified by modeling a short optical pulse passing through a zero-index slab (figure 3). The simulation reveals that the pulse propagates at the speed of light until entering the slab, where it propagates at a quarter of the speed of light, *c*/4. Causality is maintained and zero-index materials are found to support only subluminal propagation.

Further, the elimination of phase accumulation in waves propagating in a zero-index material, known as 'phase-free' propagation, is not unique to zero-index materials. This property can be most simply achieved with a periodic grating structure or 1D photonic crystal [60], and has been experimentally

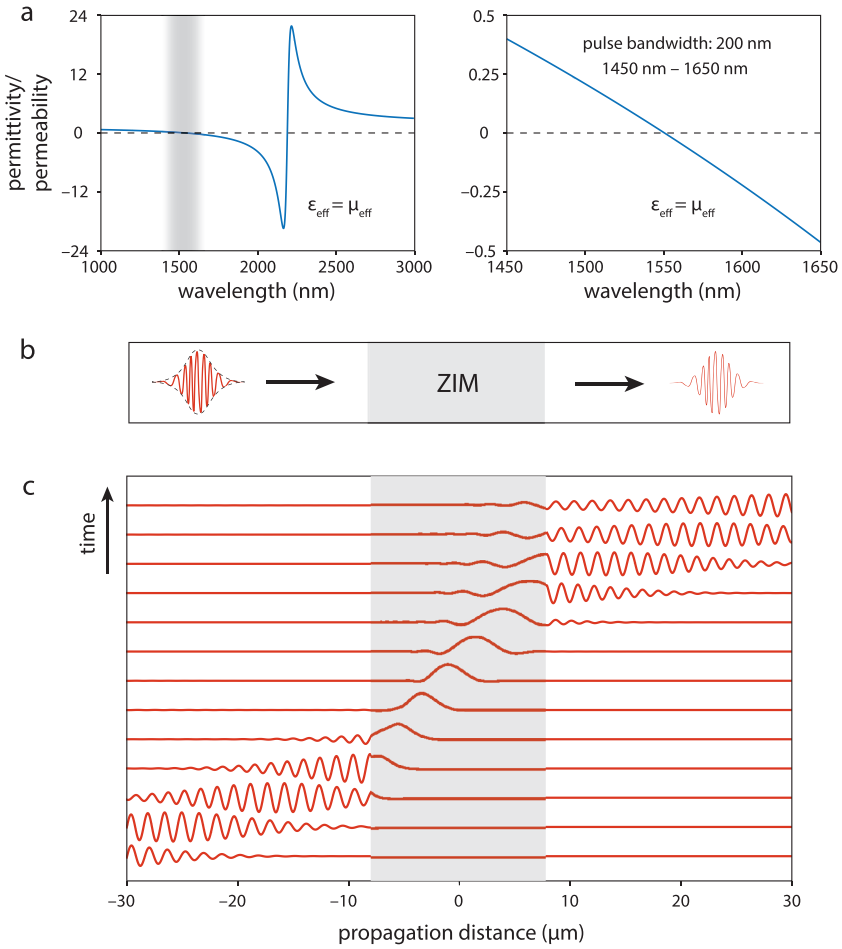

Figure 3. Causal pulse propagation in zero-index media. (a) (left) The zero-index medium is modeled as a matched pair of magnetic and electric Lorentzian oscillators. The spectra of ϵ and μ show a resonance near $\lambda = 2250$ nm, with a zero crossing at $\lambda = 1550$ nm. The shaded region indicates the bandwidth of an incident pulse (1450 nm–1650 nm). (right) The ϵ and μ within the spectrum of the pulse. (b) The transmission of a transform-limited broadband pulse (1450 nm–1650 nm) through a 16-μm-thick zero-index slab with the dispersion shown in (a). (c) Electric field amplitude of the pulse during propagation. The grey band indicates the extent of the ZIM slab. Each field profile is separated by 31 fs, which is equivalent to 6 oscillation periods at the central frequency of the pulse.

demonstrated in 2D photonic crystals as well [61]. From the perspective of a photonic band structure, this effect is equivalent to exciting a mode residing at the Γ-point of the Brillouin zone [62]. However, these standing Γ-point modes necessarily suffer from slow-light effects [63, 64]. As these modes generally reside at a band edge, they exhibit an infinite group index and are unable to transmit energy due to a resulting null group velocity. This behavior is functionally equivalent to that of ENZ and MNZ materials at their respective zero crossings [29, 65]; when the permittivity and permeability do not cross zero simultaneously (figure 4(a)), a bandgap is produced between their zero-crossing wavelengths with a corresponding imaginary refractive index (figure 4(c)). While this seemingly produces a range of frequencies associated with zero-index, enabling the aforementioned superluminal propagation, the bandgap is associated with strong dispersive loss and reflection that is maximized at the center of the gap (figure 4(d)). In contrast, when both permittivity and permeability cross zero simultaneously (figure 4(e)), the effective refractive index remains real (figure 4(f)), the band gap is closed to form the Dirac cone with a linear dispersion (figure 4(g)), and the group index remains finite over the entire operation range (figure 4(h)).

3. Design and demonstration of Dirac-cone ZIM

While Dirac-cone ZIMs enable access to zero-index properties, it is challenging to achieve the dual permittivity and permeability of zero due to weak magnetic responses in the optical regime. Understanding Dirac-cone ZIM requires exploration of Mie theory and effective medium properties, which have enabled both theoretical and experimental demonstrations for microwave and optical wavelengths in recent years. The following sections explore the physical explanation and history of Dirac-cone ZIMs.

3.1. Tuning permeability

Finite impedance and linear dispersion are intrinsic properties of Dirac-cone ZIMs that are especially suited for integration with the existing silicon photonics platform. However,

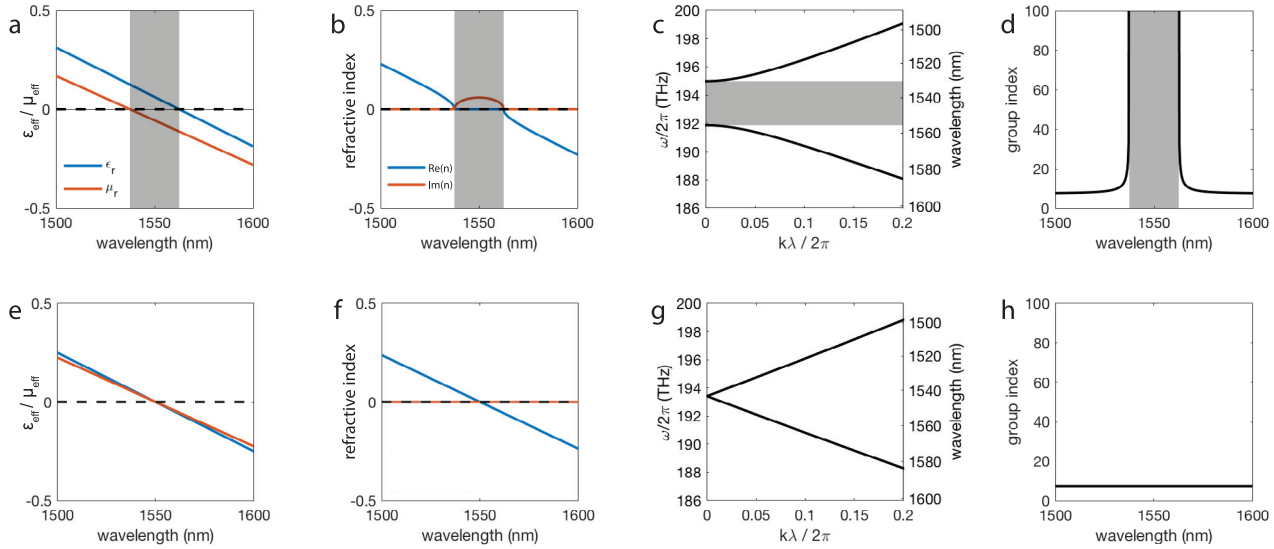

Figure 4. When the degeneracy is broken between the electric and magnetic zero-crossings (a), a band gap opens in the region where the permittivity and permeability have opposite signs ((b)–(c)). This corresponds to a diverging group index (d). However, when a perfect degeneracy is achieved (e), the gap is closed ((f)–(g)) and the group index remains finite (h).

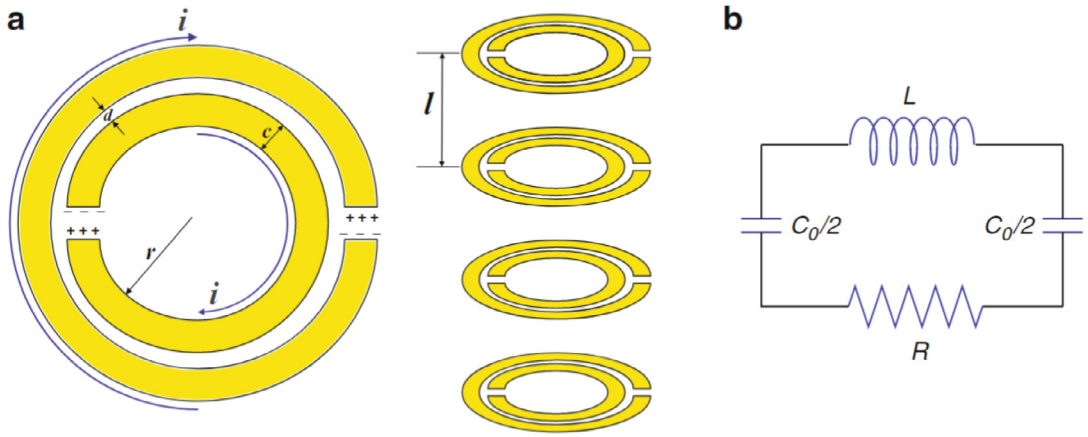

Figure 5. (a) Schematic of the double split-ring resonator used to achieve a negative permeability at microwave frequencies. (b) The equivalent LC circuit. [73] © 2010 Springer Nature. With permission of Springer.

the prerequisite condition of tuning the permittivity and permeability to zero at the same frequency is non-trivial in the optical regime. While ENZ conditions can occur in nature, permeability values other than unity are difficult to obtain due to the lack of naturally occurring magnetic resonances at optical frequencies. However, metamaterials have emerged as a common method of engineering a magnetic response at optical frequencies [66–70]. A subwavelength split-ring resonator was the initial basis for achieving variable permeability values (figure 5) [71]. The resonator consists of a metallic ring with a small gap; the ring supports a circular current that is generated in response to the magnetic component of the applied field, while a capacitance results from the charge differential across the gap. The combination of the two creates a resonant element, providing access to a range of permeability values. In response to an applied electromagnetic field, Faraday's law dictates that the circular current generated in the resonator creates a magnetic dipole that is oscillating in opposition to the applied time-varying magnetic component.

A variation of this effect is featured in every metamaterial that achieves a tunable permeability, including the first negative refractive index metamaterial [73] and many of the subsequent metal-inclusive iterations [69, 74, 75]. Negative refraction has also been demonstrated using surface plasmon polariton modes [76] and in a 3D metal-clad fishnet geometry also featuring a current loop [77–79]. The same class of structure was eventually used to demonstrate an impedance-matched zero-index metamaterial, as shown in (figure 6) [26]. As the majority of negative index metamaterials demonstrated to date incorporate metals, these metamaterials feature complex fabrication procedures and Ohmic losses, severely limiting the material thicknesses and preventing many potential applications.

Transitioning to an all-dielectric resonator requires a slightly modified approach to achieve the same tunable permeability and notably eliminates the source of optical absorption. A dielectric sphere embedded in a lower index medium supports an infinite series of frequency-dependent modes that

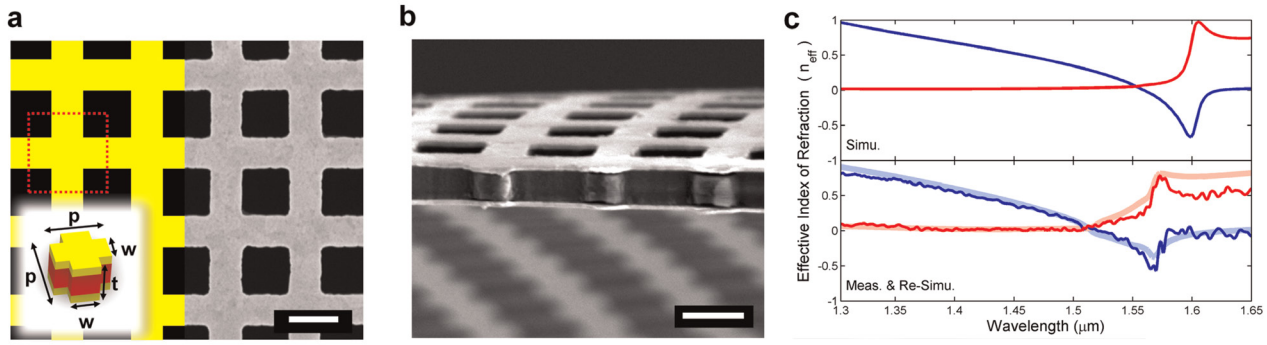

Figure 6. (a) Left: diagram of the optimized fishnet structure that produces a near zero refractive index at 1.55 μm. One unit cell is enclosed within the red dotted square. Right: top-view FESEM image of the fabricated zero-index metamaterial. Scale bar, 500 nm. (b) Cross-sectional FESEM image showing Au and polyimide layers. Scale bar, 500 nm. (c) Real (blue) and imaginary (red) parts of the inverted effective refractive index. Reprinted with permission from [26]. Copyright (2012) American Chemical Society.

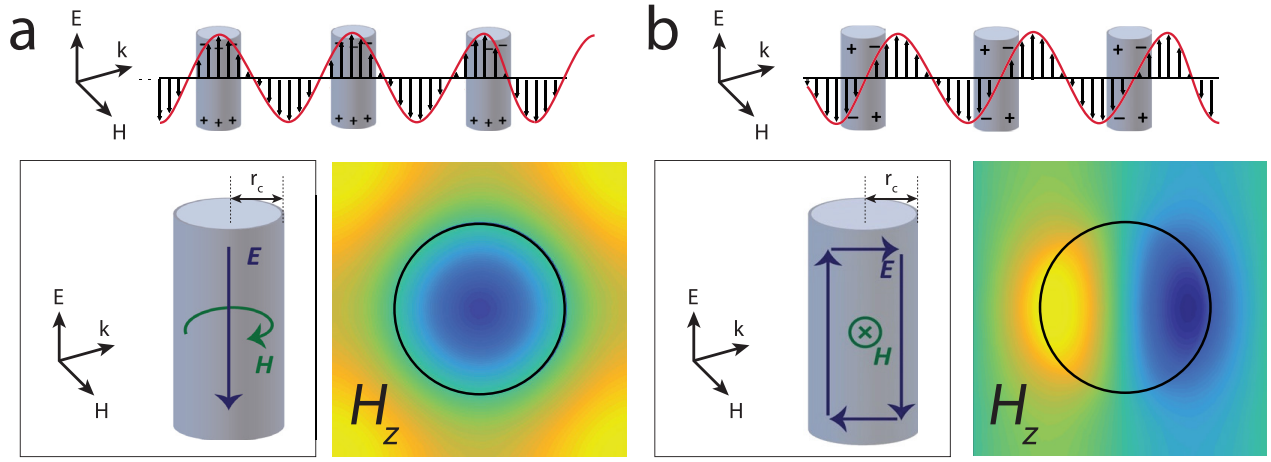

Figure 7. Light scattering from an infinitely tall dielectric cylinder can be decomposed as a series of Mie resonances. The lowest order terms are the (a) monopole mode and (b) dipole mode. The color map represents the out-of-plane electric field through a cross section of the cylinder. The electric (blue) and magnetic (green) fields in the cylinder are shown to the left of the color maps. The electric field of the incident wave is polarized along the axis of the cylinder and shown above the color maps.

can be excited by incident electromagnetic waves, creating both electric and magnetic resonances. The relative strength of these excitations is resolved through Mie scattering theory. This nomenclature can be extended to commonly include a sphere's 2D counterpart—the pillar [66, 68, 80–88]. Like the split ring resonator, Mie resonators can be combined in the form of arrays such that the collective excitation corresponds to an overall effective permittivity and permeability. These values can be calculated as a function of the geometric parameters of the resonator and were used to theoretically predict negative refractive index metamaterials consisting of dielectric spheres and rods [82, 83].

3.2. Mie theory and effective medium properties

As higher frequencies produce progressively weaker Mie resonances, all but the two lowest order modes can be disregarded when calculating the effective properties of a metamaterial. The zeroth and first order modes are found to contribute most significantly to the response of the dielectric resonator. The modes supported are polarization-dependent for a rod resonator, where transverse magnetic (TM) polarization indicates an electric field oriented along the axis of the rod, and the electric field of transverse electric (TE) polarization is oriented perpendicular to the rod. Generally, the zeroth order (TM_0) mode appears as a monopole when viewed from above and corresponds to the electric response, while the first order mode (TM_1) appears as a dipole and provides the magnetic response (figure 7). For the purposes of this review, the following discussion primarily focuses on the response of rod resonators to TM polarized light. Rods are planar fabrication compatible, and the response to TM polarized light can be translated to TE polarizations with the knowledge that the relationship is reversed: TE_0 is associated with the electric response and TE_1 is associated with the magnetic response.

The same effect that enables negative permeability values also enables access to the zero transition point between the positive and negative regimes. As such, achieving a negative or zero refractive index in a dielectric metamaterial is based on a common paradigm that relies on the combined effect of the electric and magnetic resonances. For the former, a *real* negative refractive index is only achieved if both responses have negative values. To possess a finite impedance, the zero-index case is further restricted to simultaneously zero

permittivity and permeability values. In either case, the resonances associated with the zeroth and first order modes must be overlapped such that the desired values can be achieved at a single frequency and, preferably, for the same polarization. The combination of TM_0 and TM_1 modes that achieve a negative refractive index has been studied theoretically [89, 90] and demonstrated at microwave frequencies [91]. Interestingly, many experimental demonstrations involve two different resonators separately corresponding to the electric and magnetic responses [68] and a negative index has not been achieved experimentally at optical frequencies prior to Dirac-cone ZIMs that exhibit a negative index at lower frequencies [67].

To resolve the overall electric and magnetic response of an engineered ZIM consisting of an array of dielectric pillars, an effective medium theory based on scattering cancellation in Mie resonant structures is used [92]. The design can then be verified with full-wave electromagnetic modeling by retrieving the complex reflection and transmission coefficients of the metamaterial as excited by a plane wave [93]. However, when the geometry consists of a periodic array of dielectric resonators, it becomes appropriate to use the mathematics and language developed to describe photonic crystals. Though the specific electric and magnetic responses of the resonators were not explicitly discussed, photonic crystals have been successfully treated as effective materials, including cases where the refractive index is negative [94, 95].

In fact, many results were advanced towards achieving isotropic effective media using monolithic photonic crystals [31, 32, 94, 96–99]. Remarkably, this was originally theorized in the 1950s, even predicting effective indices below unity [95]. These all-dielectric photonic-crystal-based metamaterials even featured the benefit of true isotropy within the plane of propagation as a natural consequence of a photonic crystal's symmetry.

3.3. Theoretical prediction and first appearances

Mie-based dielectric metamaterials can achieve a significant range of effective refractive indices, encompassing negative, zero, and positive values, by simultaneously engineering electric and magnetic resonances [30, 32, 92, 96]. Generally, each dielectric pillar supports a monopole (TM_0) and dipole (TM_1) mode (figure 7). To achieve the desired finite-impedance ZIM, the resonances associated with these modes are tuned to cross zero at the same frequency through variation of only two geometric parameters: the pitch (a) of the array, and the radius (r) of the pillars. When this resonance overlap occurs, the associated modes can be considered degenerate; operation at the same frequency produces a field that oscillates between the two. In terms of the photonic band structure, this degeneracy manifests as a Dirac-cone dispersion at the center of the Brillouin zone [30–32]. The characteristic cone results from two curved bands joining, the occurrence of which creates a linear dispersion for a range of frequencies in the vicinity of the overlap frequency. The photonic analog to the dispersion of graphene features this intersection of two linear bands, and an additional 'flat' band at the center of the Brillouin zone (figure 8(a)). The two linear bands correspond to hybridizations of the monopole and dipole modes, whereas the flat band corresponds to the dipole mode in a rotated orientation typically inaccessible from normal incidence. The presence of the flat band is a necessary consequence of isotropy, as the material must behave consistently regardless of excitation direction along the square lattice.

As the Dirac cone is located at the Γ-point, the three modes that are encompassed feature zero phase-advance. While isotropic, the monopole mode cannot be excited by a plane wave source as a result of symmetry mismatch. Instead, the dipole mode is responsible for the non-zero group velocity. A ZIM that features this dispersion profile oscillates between the monopole and dipole modes when operated at the zero-index frequency, supporting energy transmission through the propagating hybridized mode [96]. Further, as the Dirac-cone dispersion resides above the light line due to its position at the Γ-point, ZIMs inherently exhibit radiative loss [44] while the same dispersion positioned elsewhere in the lattice has the potential to be confined but eliminates the zero phase advance property [6, 38].

A Dirac-cone ZIM was first demonstrated in the microwave regime by Huang *et al* in 2011 [30] using a square array of alumina rods embedded within a parallel-plate waveguide (figures 8(a) and (b)). The inclusion of a parallel plate structure serves as a perfectly electric conductor (PEC) boundary, or a mirror that effectively confines the leaky zero-index modes in the out-of-plane direction. Using this implementation, the authors demonstrated cloaking and lensing effects enabled by a zero refractive index. It is notable that a Dirac-cone ZIM has also been demonstrated at lower, acoustic frequencies, enabling the first experimental visualization of the Dirac-cone dispersion [100].

3.4. Optical ZIM

Achievement of a Dirac-cone ZIM at microwave frequencies naturally inspired efforts toward scaling the metamaterial to optical frequencies. The first Dirac-cone metamaterial at optical frequencies was demonstrated by Moitra *et al* in 2013 [33]. The geometry of the structure deviated from a 2D photonic crystal and was instead consisting of a horizontal array of silicon pillars, more closely resembling that of a fishnet metamaterial (figures 8(c) and (d)). This work was especially crucial as it revealed that the reflective PEC boundary was not necessary and that the refractive index of silicon was sufficiently high to support the necessary modes. However, the fishnet geometry relies on out-of-plane excitation, incompatible with integrated devices. The interaction distance is limited as the number of unit cells in the propagation direction is dependent upon a high aspect ratio etch.

An integrated platform more closely resembling the photonic crystal format was demonstrated in 2015 by Li *et al* [34]. This ZIM was the first to enable in-plane propagation compatible with existing integrated photonic elements, such as waveguides and resonators. A metal cladding was used to

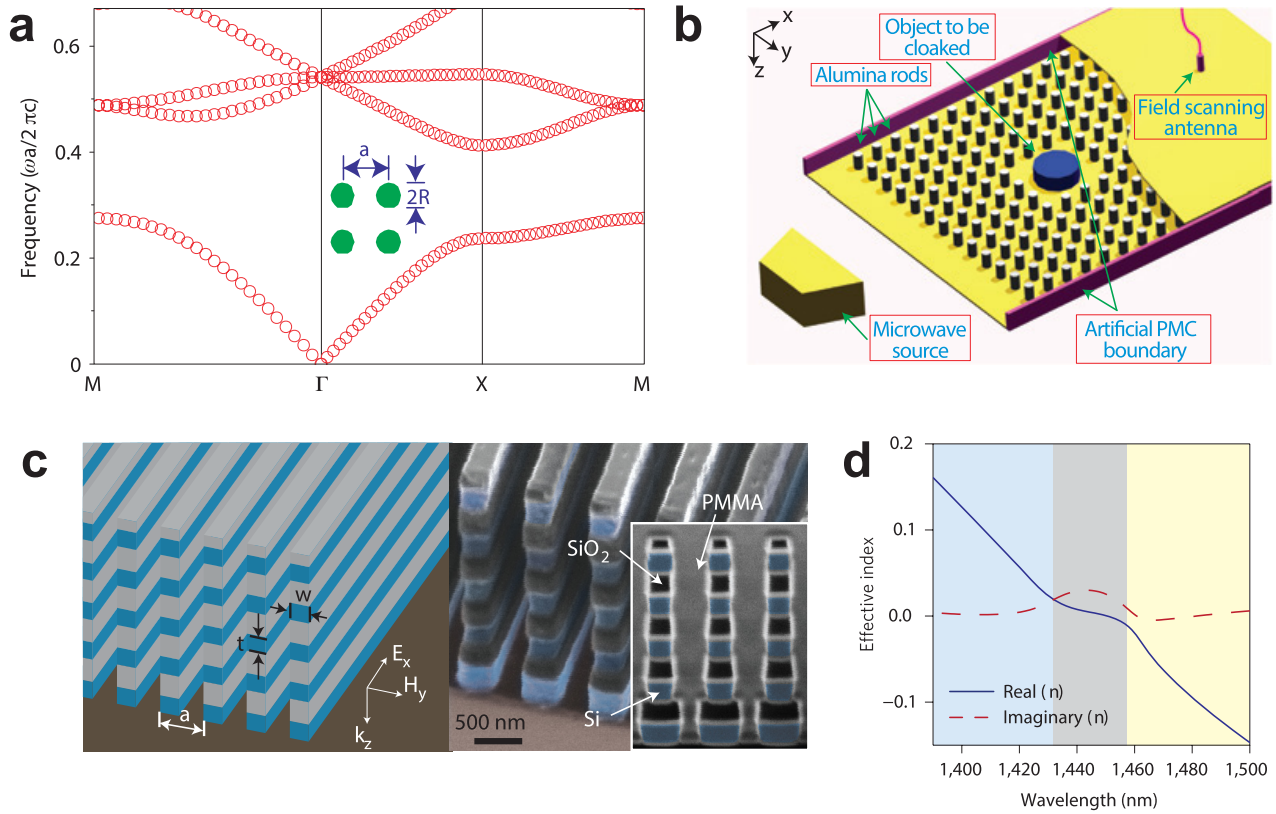

Figure 8. (a) The photonic band structure of a photonic crystal consisting of a square lattice of infinitely tall silicon pillars with radius $r = 0.2a$, relative $\epsilon = 12.5$ and relative $\mu = 1$. The two linear bands intersect to form a Dirac cone at $f = 0.541c/a$. (b) This first Dirac cone metamaterial was demonstrated in the microwave regime using a square array of alumina rods. (c) A schematic and colored SEM of a Dirac cone zero-index metamaterial based on a horizontal square array of silicon bars that operates in the infrared. (d) The experimental real and imaginary component of the effective index for the structure in (c). Reprinted by permission from Macmillan Publishers Ltd: Nature Materials [30], Copyright (2011). Reproduced permission from Macmillan Publishers Ltd: Nature Photonics [33], Copyright (2013).

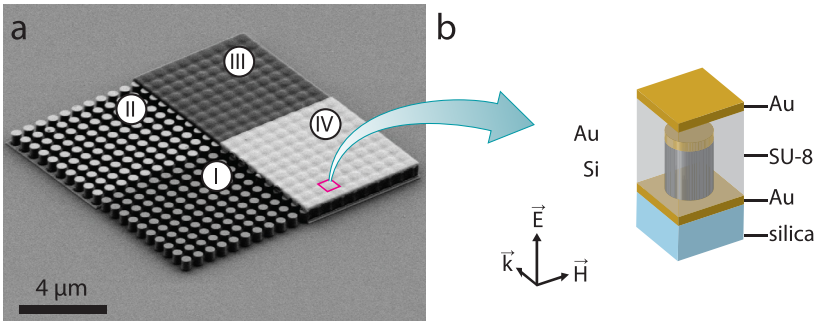

Figure 9. Metamaterial structure of original integrated platform. (a) Scanning electron microscope image of the fabrication procedure: (I) the pillar array is patterned via e-beam lithography and structured via reactive ion etching, (II) a bottom gold layer is deposited via electron beam evaporation, (III) the pillars are embedded in a polymer matrix, (IV) a second evaporation deposits a top gold layer. (b) Designed unit cell. Adapted with permission from Macmillan Publishers Ltd: Nature Photonics [34], Copyright (2015).

make the pillars appear optically infinite in order to emulate the behavior of 2D pillars. The cladding further acted as a PEC boundary, identical to the PEC included in the microwave demonstration [30]. The ZIM could be lithographically patterned in arbitrary shapes, circumventing the previous limitation of short interaction lengths, crucial for applications in nonlinear optics [13] and field enhancement [101].

Although the metal-clad ZIM was compatible with planar fabrication techniques, it had significant flaws that hindered the possibility of widespread adoption. Notably, the metal layers reintroduced resistive losses originally intended to be avoided in Dirac-cone ZIMs. Furthermore, the fabrication procedure is prohibitively complex, limiting repeatability (figure 9).

To make ZIMs more attractive for potential applications, future iterations emphasized simplification of the metamaterial structure. Since this initial demonstration of an integrated ZIM (which will be referred to as metal-clad ZIM), there have been two additional experimental Dirac-cone ZIM implementations consisting of just structured silicon-on-insulator (SOI) and surrounding air: (1) silicon pillars in air [36, 46] for TM-polarized light (this will be referred to as

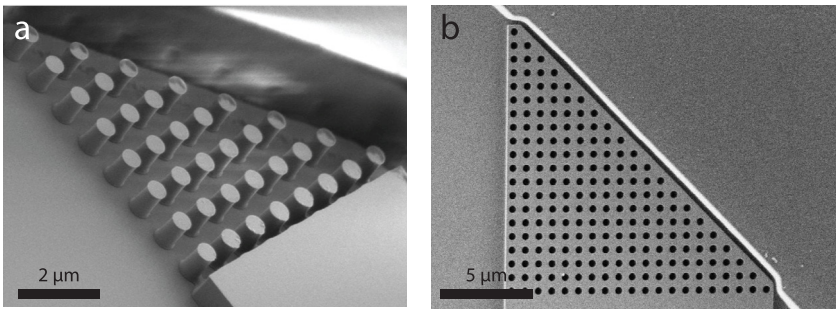

Figure 10. SEM images of zero-index metamaterials fabricated in a prism device. (a) Silicon pillars in air prism. (Reproduced from [36]. CC BY 3.0. © 2017 Optical Society of America.), (b) Air hole in silicon matrix prism. Reproduced from [37]. CC BY 3.0. © 2017 Optical Society of America.

pillar ZIM), and (2) the complementary structure of air holes in a silicon matrix [37] for TE-polarized light (this will be referred to as air hole ZIM). Both ZIMs can be fabricated in a single e-beam lithography step (figure 10).

4. Challenges of Dirac-cone ZIM

While the initial fabrication challenges have been largely resolved, there remain some notable obstacles to the widespread adoption of Dirac-cone ZIMs. The prerequisite modal degeneracy is extremely sensitive to any fabrication deviations or imperfections. Since most Dirac-cone ZIMs are based in a pillar resonator for TM excitation, it is difficult to use thinner device layers that are more compatible with single mode waveguides. Further, while reactive ion etching is an anisotropic procedure, generally gently sloped sidewalls often result; the typically high aspect ratio of pillar resonators accentuates the effect of the slight angle in the etch profile. Radiative losses are inherent to Dirac-cone ZIMs and are a significant obstacle to creating devices with long propagation lengths or large areas. These losses also contribute to deviations from the desired linear dispersion. Finally, as the unit cell of Dirac-cone ZIMs is often on the same order as the operating wavelength, categorization as a homogeneous bulk is challenging and merits additional consideration. However, many of these obstacles are not intrinsic to zero-index materials and may be resolved in the near future. The following sections explore the major challenges and offers potential solutions.

4.1. Tolerance to fabrication imperfections and tunability

A significant obstacle for ZIMs is their low tolerance for parameter variation in fabrication. As the Dirac-cone dispersion results from the perfect tuning of two resonances, even a slight deviation in the fabricated dimensions can result in a breakdown of the desired behavior, producing a photonic bandgap. The tolerable variation in parameter dimension is below a percent [30], creating an obstacle towards the wide-scale adoption of a Dirac-cone metamaterial. However, it should be emphasized that a sensitivity to fabrication imperfections is characteristic of many core integrated photonics components, including waveguides and resonators [102], and not necessarily limited to photonic crystal structures. Rather, the challenge comes from the narrow bandwidth of the zero crossings of permittivity and permeability resonances.

Deviations in fabricated dimensions are particularly apparent in pillar radii, which are affected by processing conditions such as resist thickness, beam current drift and development temperature; conversely, device height and relative pillar placement (or pitch) are relatively insensitive to processing. Systematic variation in pillar radius will detune the zero-crossing of the electric and magnetic resonances, breaking the degeneracy.

Pillar structures that approach or exceed 1 μm in height have been used successfully as the constituent resonator in Dirac-cone ZIMs [36, 46]. In Kita *et al*, these relatively tall pillars were able to further demonstrate unprecedented tolerance to fabrication imperfections. Generally, to achieve a robust modal degeneracy, the two modes must possess not only identical zero-index frequencies, but their wavelength shift must also have the same dependence on structural variation (i.e. $\Delta\lambda/\Delta r$) (figure 11). The modal equivalent index (MEI) becomes useful in designing robust ZIMs as it correlates with this dependence. Defined as a sum of all constituent unit cell refractive indices weighted with respect to their field confinement [103], the MEI offers an additional parameter of consideration in achieving tolerance to fabrication imperfections. If the MEI of the two modes can be designed to remain equivalent for a range of radii, the degeneracy is expected to be maintained within this range, as well.

Independent adjustment of the modal confinement necessitates a third degree of freedom. For pillar ZIM as demonstrated by Kita *et al*, this is the silicon device thickness. Through the additional tuning of the pillar height, in addition to the original two lattice parameters (i.e. pitch a and radius r), zero-index frequency and matched MEI can be simultaneously achieved for a range of radii. The optimized metamaterial maintains zero-index operation despite radius variation of $\pm 3.6\%$, or up to ± 19 nm, corresponding to an order of magnitude reduction in sensitivity. In exploiting this modal dispersion, an increase in pillar radius results in a redshift of the zero-index frequency instead of the typical emergence of a band gap (figure 11).

While pillar ZIM significantly simplifies the fabrication procedure of the metal-clad ZIM presented by Li *et al* [34], it requires either a silicon regrowth technique or uncommonly thick device layers in order to achieve the necessary pillar

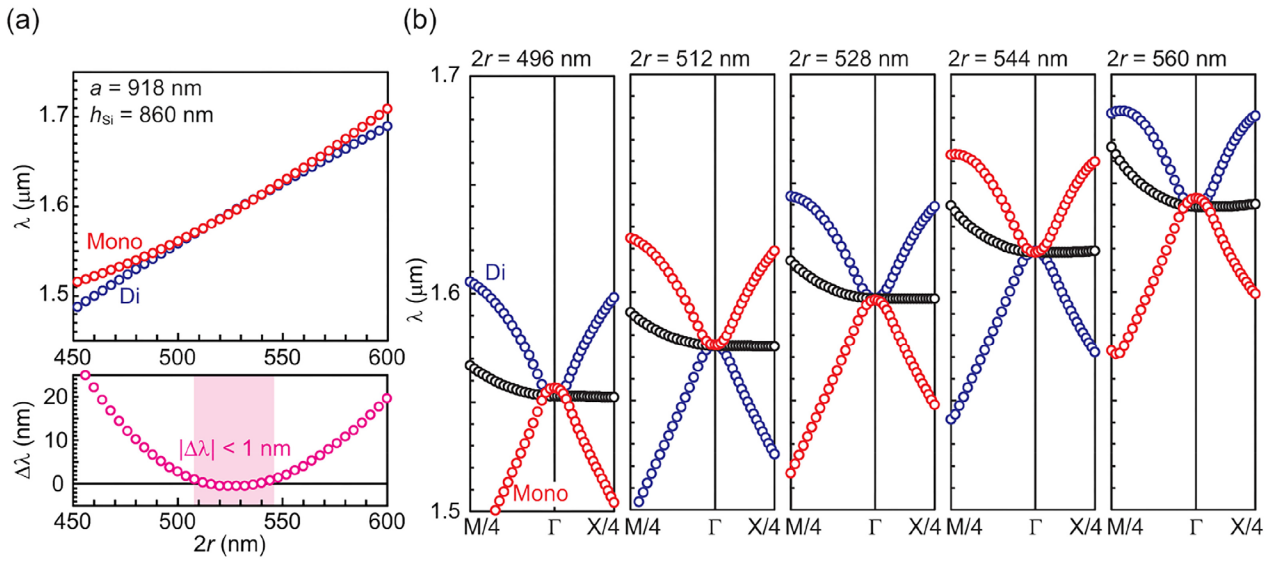

Figure 11. Fabrication-imperfection-tolerant zero-index metamaterial. (a) (top) Resonant wavelengths of the monopole (red dots) and dipole (blue dots) modes, with dimensions of the unit cell shown in the top left of the graph. (bottom) The difference $\Delta\lambda$ in resonant wavelengths between the two modes with respect to variations in pillar radius r. (b) Photonic band structure for a range of radii showing the Dirac-cone degeneracy at different wavelengths. The red and blue bands are now understood to be hybridized modes rather than associated with only the monopole or dipole modes, respectively. Black dots indicate the rotated dipole mode. Reproduced from [36]. CC BY 3.0. © 2017 Optical Society of America.

height; taller device layers often prevent single mode operation in coupling structures. However, the concept is transferable to any metamaterial that allows for control of modal dispersion in its constituent resonators. One obvious variation is core shell, or 'coated' resonators that adds parameters associated with a coating or void [104, 105] and has been used to theoretically demonstrate Dirac cone zero-index [106–108]. However, alternate lattices [55, 106–109] or malleable substrate materials [110] may provide promising solutions as well.

Without the addition of a degree of freedom, it is challenging to achieve fabrication-tolerant ZIMs. However, post-fabrication tuning methods are available. Mechanical strain can tune the distance between resonators and index matching fluid is commonly used to adjust the refractive index of the background medium. Finally, thermal tuning, either through application of heat directly or by powering metallic inclusions on chip, has long been used for fine tuning after fabrication is complete.

4.2. Device height

The Dirac-cone dispersion originates in infinitely tall silicon pillars [30, 32, 33, 96] making the realization of a ZIM with a finite height challenging. Attempts to approximate an infinite pillar height have included the addition of a metal-cladding such that the pillars appear optically infinite [34], and use of pillars with high aspect ratio geometries [33, 36, 46]. However, the former involves a prohibitively complex fabrication procedure and the latter introduces incompatibility with common coupling structures and standard SOI device heights. While achievement of a ZIM has a significant dependence on pillar height, compatibility with existing integrated platforms limits heights to those available in commercial silicon-on-insulator (SOI) wafers with lower device thicknesses. This is particularly challenging for the TM modes associated with dielectric pillars as there is a stricter dependence on minimum height necessary to support the modes [111, 112].

To significantly reduce the aspect ratio of the metamaterial, the amount of confining material can be increased. Vulis *et al* [37] achieved this by increasing the volume filling fraction of silicon as compared to air: the unit cell design is inverted, transitioning from silicon pillars in air to air holes in a silicon matrix [37]. The air hole ZIM is fabricated using a 220-nm silicon device layer, a significant reduction from the pillar ZIMs that required a device height of 500 nm or greater. In contrast to the pillar metamaterial, the air hole ZIM is designed for TE polarized light. This polarization is found to offer improved confinement for thinner device layers [60, 113].

While this design still achieves a Dirac-cone dispersion, the degenerate modes exhibit a higher order of symmetry; instead of the monopole and dipole modes of the pillar ZIMs, this air hole ZIM features the degeneracy of dipole and quadrupole modes. While Dirac cone ZIMs involving higher order modes had been predicted [39, 96], the air hole ZIM represents the first experimental demonstration of this specific degeneracy.

While the same experimental result is achieved, higher order modes are generally disadvantageous due to the resulting weaker resonances. While theoretically possible, most high order modes cannot be experimentally achieved. However, the inverse structure of a air hole ZIM cannot be mapped to the pillar resonances commonly associated with Mie-based metamaterials as it is not expected to support a monopole mode in a low index void. Ashraf *et al* [108] report that a Dirac cone ZIM achieved through a core shell structure results from the degeneracy of monopole and dipole modes when the coating possess a lower refractive index than the core, while inverting the coating and the core results in a degeneracy of the

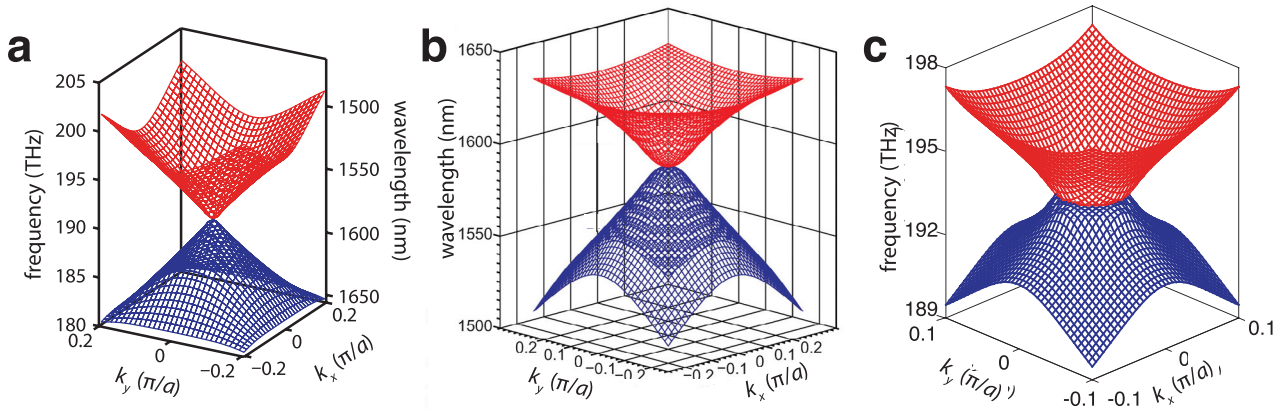

Figure 12. Three-dimensional dispersion surfaces of different zero-index metamaterials. Band structure of (a) metal-clad platform with the linear bands (blue) forming a Dirac-cone and an additional flat band (red). (b) silicon pillar in air platform and (c) air hole in silicon matrix platform with top portion of the band shown in (red) and bottom portion in (blue). The flat band is removed for clarity. Adapted with permission from Macmillan Publishers Ltd: Nature Photonics [34], Copyright (2015). Reproduced from [36]. CC BY 3.0. © 2017 Optical Society of America. Reproduced from [37]. CC BY 3.0. © 2017 Optical Society of America.

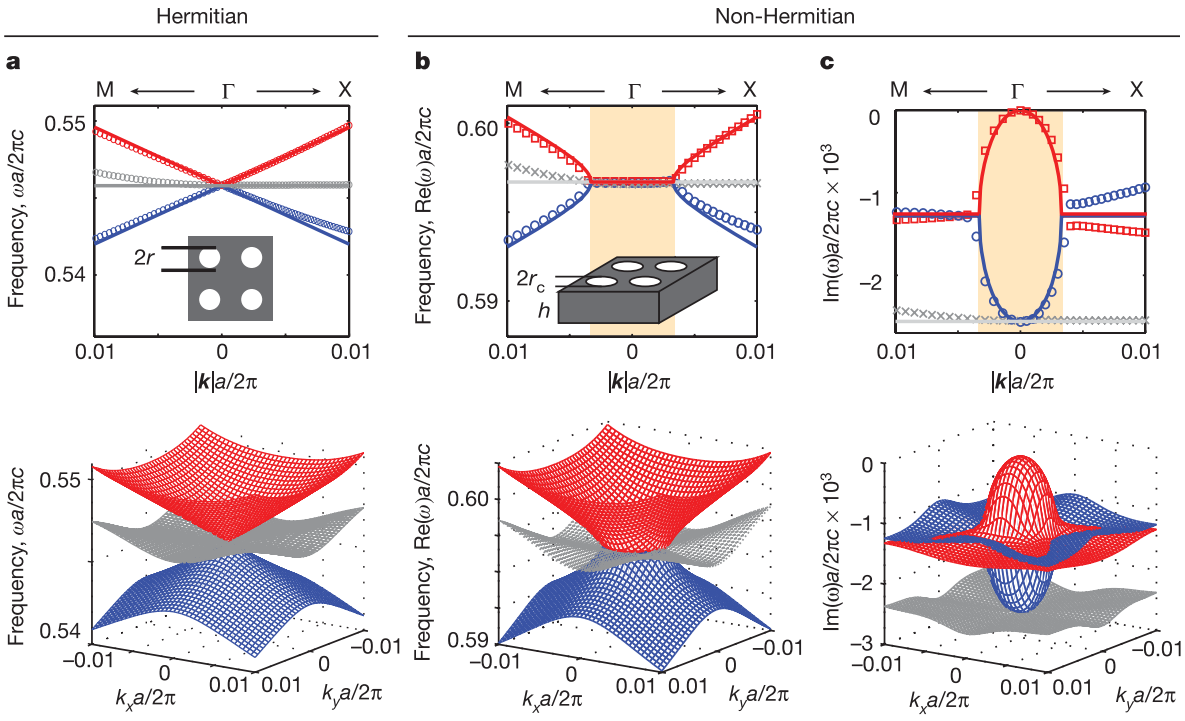

Figure 13. Accidental degeneracy in Hermitian (lossless) and non-Hermitian (lossy) photonic crystals. (a) Band structure of a 2D photonic crystal consisting of a square lattice of circular air holes. Tuning the radius r leads to accidental degeneracy producing two linear bands with (red and blue) and an additional flat band (grey). The (b) real and (c) imaginary parts of the eigenvalues of a photonic crystal slab with finite thickness, h. Reprinted by permission from Macmillan Publishers Ltd: Springer Nature [39], Copyright (2015).

dipole and quadrupole modes, further confirming this result. However, a degeneracy incorporating a quadrupole mode may be the limit of modal order that can be achieved experimentally without higher refractive index materials. The quadrupole in particular features a node at its center which may offer an advantageous placement option for emitters or other point sources. Intentional selection of higher order modes has been theoretically demonstrated in a polarization-independent ZIM by Lin *et al* where the field distribution of the modes is used as a starting condition instead of a consequence [114].

4.3. Modal degeneracy and band structure

While all integrated ZIMs are based on a Dirac-cone dispersion [30], full-wave simulations reveal subtle differences in the resulting dispersion surfaces at the degeneracy. Fundamentally, all designs feature the intersection of two bands corresponding to the degeneracy of the dipole and monopole modes (or quadrupole, in the case of the air hole ZIM), and a third flat band corresponding to the rotated dipole mode (figure 12). While the metal-clad ZIM has a linear dispersion

near the Dirac point, the two all-dielectric platforms show a slight quadratic dispersion at the intersection. This deviation from linear begins to emulate a ring of exceptional points. The relation between Dirac cones and exceptional points has been previously theorized [115, 116] and recently demonstrated in a photonic crystal slab [39]. The demonstrated all-dielectric Dirac-cone zero-index metamaterials can be argued to possess either a Dirac-cone or exceptional point dispersion. These can be considered as equivalent as in the latter case; the degeneracy is tuned such that the ring radius is negligible as compared to seemingly flattened dispersion (figure 13)—effectively forming the single point degeneracy.

Generally, a quadratic dispersion is undesirable. As the slope of the band is directly correlated with the group velocity, a quadratic dispersion would result in components of an applied pulse signal propagating through the ZIM at different speeds, producing distortion. The source of this quadratic dispersion originates from the difference in radiation of the two degenerate modes. By contrast, the dipole mode in a 2D system cannot access an out-of-plane radiation channel, resulting in a perfectly linear cone. [39]; the introduction of loss channels (for example, with a finite device height) causes the dispersion to curve near the degeneracy. This is an unfortunate consequence of ZIMs as the Dirac cone degeneracy lies above the light line and, as such, its constitutive modes are intrinsically radiative [60].

The degree of radiation is strongly related to the compatibility of the modal symmetry with a plane wave. The monopole and quadrupole modes possess symmetries incompatible with a plane wave. This is not the case with the symmetry of dipole modes. The quality factor of the monopole and quadrupole are found to be several orders of magnitude higher than that of the dipole mode [34, 36, 37]. This loss channel primarily driven by the dipole mode results in a lower group velocity in the vicinity of the Dirac cone and the resulting quadratic dispersion [39, 117].

However, the plane-wave nature of the radiation enables a method of confinement through the interference of loss channels. In the band structure of metal-clad ZIM, the dispersion is noticeably linear. This linearity results from the metal cladding, which reduces the quality factor of the monopole mode through absorptive losses, while the addition of a mirror limits the expected radiation of the dipole mode. Therefore any similar method of confinement should be expected to match the loss of the degenerate modes more closely and achieve a linear dispersion (see *Losses*).

The losses introduce a secondary complication in the interpretation of the band structure. Whenever losses are present in the system—either from material absorption or radiation—an ambiguity arises in the computation of band structure. These losses introduce imaginary components that cannot be fully portrayed in a 2D band structure. There are therefore two branches of solutions: the eigenmodes of the system with real propagation wavevectors ($\vec{k}$) and complex operating frequencies (ω) (as typically provided by commercial eigenmode solvers using the finite element method), or the inverse case of entirely real ω and complex $\vec{k}$ (as typically produced by finite-difference time-domain methods) [118, 119]. Typically,

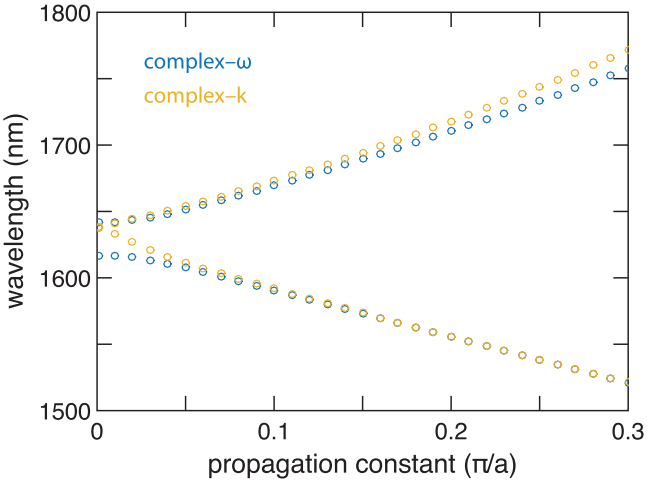

Figure 14. Complex-$\vec{k}$ and complex-ω solutions to the band structure of a zero-index waveguide, the 1D analog [120] of the air hole ZIM [37]. When computed using the standard complex-ω method, the mode degeneracy is obfuscated.

losses are small enough that the differences between these two methods are negligible.

However, this is not the case for Dirac cones dispersions. Firstly, a Dirac cone ZIM is dependent on achieving a degeneracy of two modes which can be obscured if the incorrect simulation method is used (figure 14). Secondly, due to their location above the light line in the Brillouin zone, these modes possess significant imaginary components reflective of their leaky nature. Third, the difference in quality factor of the degenerate modes (See *Modal degeneracy and band structure*) indicates that each mode possesses different imaginary values that further confound the results.

As modes in any photonic crystal are excited using lasers corresponding to real ω, and losses are primarily accumulated with propagation, the complex-$\vec{k}$ simulation approach is expected to yield results that more closely resemble experimental conditions [118, 119].

4.4. Treatment as a homogeneous material

The treatment of a material with a Dirac-cone dispersion as an effectively zero-index medium has been both a challenge and a point of debate in recent years [99, 121] due to its origin as the degeneracy of multiple modes. An ideal, fully homogeneous metamaterial should support a single propagating mode at the wavelength of operation; otherwise ambiguity is introduced in assigning a refractive index. Dirac-cone metamaterials, however, are based on the degeneracy of three modes at the zero-index frequency: a monopole or quadrupole, and two dipole modes. The result is an additional flat band that intersects the Dirac cone that constitutes a second mode in the strictest homogenization consideration [121].

However the symmetry of the modes plays a significant role in its relevance. Therefore, it may be possible to describe Dirac-cone metamaterials by an effective index for a subset of illumination conditions. In this case, we may treat the hybridized behavior of the two degenerate modes at the zero-index frequency as a single mode. While the third band,

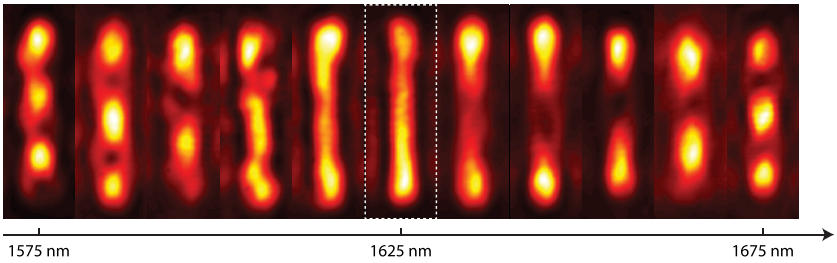

Figure 15. Standing wave patterns resulting from the interference of two counter-propagating sources in a ZIM waveguide for wavelengths ranging from 1575 nm to 1675 nm. The extension of a node across the entire length of the ZIM waveguide indicates effectively homogeneous zero-index behavior at normal incidence. Reprinted with permission from [121]. Copyright (2017) American Chemical Society.

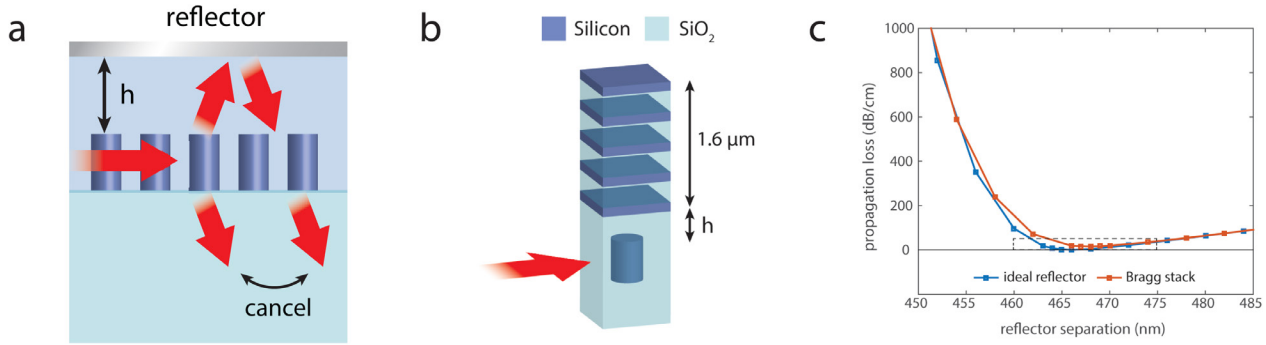

Figure 16. Effect of adding a reflector to form a bound state in the continuum. (a) Schematic showing example reflector placement to contain upward radiation such that it destructively interferes with the downward radiation. (b) Schematic of Bragg reflector design used to produce the propagation loss results shown in (c) as compared to an ideal reflector.

corresponding to the longitudinal dipole, is incompatible with incident plane waves, its effects cannot be completely ignored as it is possible to excite the longitudinal dipole via oblique or evanescent waves, introducing undesirable coupling that is inconsistent with the behavior of an effective medium. Excitation of the longitudinal dipole can be avoided for normal incident illumination or through operation at a frequency slightly above the degeneracy. As such, while the ZIM can behaves similarly to an ideal zero-index material, it is inaccurate to describe it as homogeneous in the strictest sense. By characterizing the conditions for single-mode operation, the limitations in application of Dirac cone ZIM cone can be identified.

For treatment as a homogeneous medium, the material must satisfy the additional criteria of isotropy, passivity, causality, and lack of radiative and scattering losses [122]. The passivity criterion is easily satisfied by using a low-loss dielectric material. Superluminal pulse propagation is not possible and causality is maintained (*see dispersion and causality*). The presented ZIMs generally exhibit a significant isotropic bandwidth around the Dirac-point (55 nm for the pillar ZIM, and 20 nm for the air hole ZIM [34, 37]). The radiative and scattering loss criterion, however, is problematic and worthy of additional discussion. This criterion refers not only to direct losses, but also those incurred from coupling to additional modes. Due to the presence of additional bands, this is a possibility in fabricated zero-index Dirac-cone metamaterials. Finally, the lattice constant must be sufficiently small relative to operating wavelength to avoid diffraction at the interface of the material. As the unit cells of these ZIMs are often relatively large with respect to the free space wavelength ($\approx 0.5\ \lambda$), diffraction producing non-normal components is possible.

A particularly illustrative example is the response of the ZIM to an oblique source of excitation. In general, a homogeneous zero-index material can be expected to emit light at normal incidence from each of its facets. The inverse is also true: light is expected to only enter a homogeneous zero-index material normal to the interface. However, excitation at various angles of incidence often reveals extraneous transmission at angles beyond the normal. This indicates access to modes beyond the desired hybrid degenerate mode, albeit at other angles of incidence. In the case of a metal-clad ZIM, the extraneous transmission largely results from coupling into the flat band mode and is significantly reduced by operation at a frequency above the degeneracy.

Systematic analysis of these extraneous band structure modes reveals that certain bands are inaccessible and, as such, can be neglected under normal incidence [37]. However, Dirac-cone ZIMs are not strictly consistent in behavior across a range of incident angles and coupling to these additional modes may be problematic for certain applications.

The homogeneous behavior of ZIMs at normal incidence is further verified in recent work by Reshef *et al* [120]. Although previous demonstrations of ZIMs focused on 2D unit cell arrays, the same exotic phenomena can be realized in 1D waveguides that are extremely compatible with integrated photonics. Inspired by air hole ZIM [37] and adapted to a corrugated waveguide form-factor, this waveguide supports only a single mode that propagates with no phase-advance and a finite group index. As excitation of the ZIM waveguide is

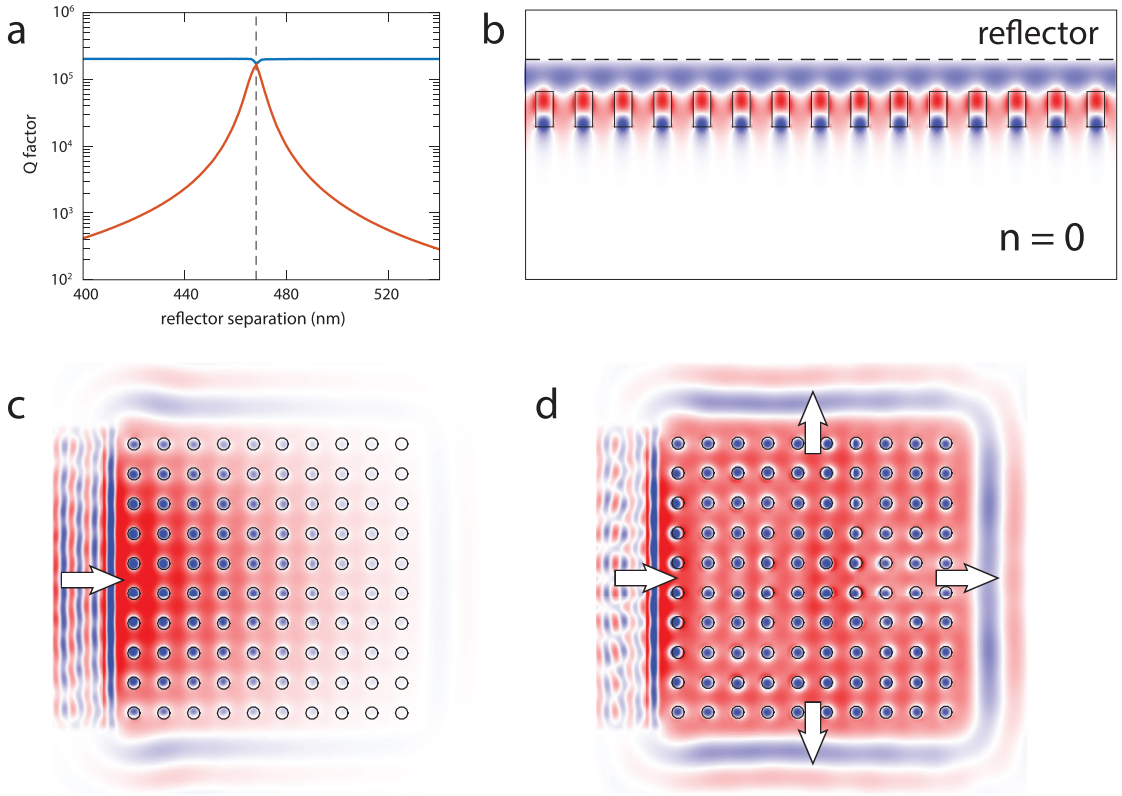

Figure 17. (a) Comparison of dipole (red) and monopole (blue) quality factors showing that they are matched for a single reflector separation height. This eliminates the dipole loss channel. (b) Effect of reflector addition on Dirac-cone ZIM as viewed from in-plane. No radiation is seen above the reflector or below the metamaterial. (c) Comparison of the fading field strength in a typical, lossy ZIM as it propagates across a large area to a (d) ZIM incorporating a bound state in the continuum that achieves even field strength across the propagation area.

normal to the interface, the observation of the standing wave pattern extended across the device and without additional interference serves as proof that indeed only the zero-index mode is accessed at normal incidence (figure 15).

4.5. Losses

Zero-index phenomena, characterized by long wavelength and spatial coherence, are primarily relevant over long propagation lengths. Therefore, loss control is paramount. The emergence of Dirac-cone ZIMs eliminate material absorption; however these metamaterials necessarily suffer from radiative loss as the constitutive degenerate modes propagate with zero momentum at the Γ-point, well above the light line.

It is possible to create resonances of open systems that do not radiate. There has recently been renewed interest in such bound states in the continuum for photonic systems [123]. Rather than using traditional methods of confining light using total internal reflection or photonic band gaps, these embedded eigenmodes eliminate radiation via destructive interference between two or more loss channels. This phenomenon was recently observed experimentally in photonic crystals [123] and can be used to eliminate propagation loss in ZIMs, enabling large area devices [124].

For example, we can eliminate radiative loss from a zero-index pillar array by introducing a reflector (figure 16). Placed above the array, the mirror reflects the leaky wave back down into the pillars, where it destructively interferes with the leaky wave below the array. The relative phase of the two overlapping waves is determined by the separation between the pillars and the reflector. Therefore, the separation can be tuned to exactly cancel the waves through destructive interference. As a result, the radiative loss is completely extinguished (figure 17), and the zero-index mode is able to propagate over long distances with reduced losses on the order of a few decibels per centimeter; in contrast, previous integrated ZIMs experience losses of approximately 1 dB μm^{-1} [34, 36, 37, 120].

5. Outlook

Dirac-cone ZIMs enable a refractive index of zero and permit the associated phenomena to be accessed, utilized, and potentially commercialized. Through integration with popular on-chip platforms such as silicon photonics, these metamaterials comprise a platform that can be easily adapted and that offers significant modularity. This review covered the history and implementation of these Dirac-cone ZIMs, and their associated design challenges. Many of these challenges can be

addressed with current methods to implement a truly accessible platform. Because these metamaterials can be implemented in an in-plane, waveguide-compatible configuration, they have the potential for significant impact in the field of integrated photonics and find varied applications, including supercoupling, beam steering, and enhancement in nonlinear optics.

Acknowledgments

The authors thank Michael Lobet, Yang Li, and Peter Saeta for helpful discussions and assistance with the reviewed work, as well as our close collaborators, Shota Kita and Marko Lončar.

ORCID iDs

Daryl I Vulis https://orcid.org/0000-0002-9225-2621
Orad Reshef https://orcid.org/0000-0001-9818-8491

References

[1] Miller D A B 2009 *Proc. IEEE* **97** 1166–85
[2] Miller D A B 2000 *Proc. IEEE* **88** 728–49
[3] Engheta N 2013 *Science* **340** 286–7
[4] Liberal I and Engheta N 2017 *Nat. Photon.* **11** 149–58
[5] Schilling J 2011 *Nat. Photon.* **5** 449–51
[6] Bravo-Abad J, Joannopoulos J D and Soljačić M 2012 *Proc. Natl Acad. Sci. USA* **109** 9761–5
[7] Chua S L, Lu L, Bravo-Abad J, Joannopoulos J D and Soljačić M 2014 *Opt. Lett.* **39** 2072–5
[8] Silveirinha M G and Engheta N 2007 *Phys. Rev. B: Condens. Matter* **76** 1–17
[9] Silveirinha M and Engheta N 2006 *Phys. Rev. Lett.* **97** 157403
[10] Mahmoud A M, Liberal I and Engheta N 2017 *Opt. Mater. Express* **7** 415–24
[11] Hao J, Yan W and Qiu M 2010 *Appl. Phys. Lett.* **96** 101109
[12] Nguyen V C, Chen L and Halterman K 2010 *Phys. Rev. Lett.* **105** 233908
[13] Suchowski H, O'Brien K, Wong Z J, Salandrino A, Yin X and Zhang X 2013 *Science* **342** 1223–6
[14] Alam M Z, De Leon I and Boyd R W 2016 *Science* **352** 795–7
[15] Argyropoulos C, DAguanno G and Alù A 2014 *Phys. Rev. B: Condens. Matter* **89** 235401
[16] Reshef O, Giese E, Zahirul Alam M, De Leon I, Upham J and Boyd R W 2017 *Opt. Lett.* **42** 3225–8
[17] Pendry J, Holden A, Stewart W and Youngs I 1996 *Phys. Rev. Lett.* **76** 4773–6
[18] Rotman W 1962 *IRE Trans. Antennas Propag.* **10** 82–95
[19] Vesseur E J R, Coenen T, Caglayan H, Engheta N and Polman A 2013 *Phys. Rev. Lett.* **110** 013902
[20] Naik G V, Kim J and Boltasseva A 2011 *Opt. Mater. Express* **1** 1090–9
[21] Feigenbaum E, Diest K and Atwater H A 2010 *Nano Lett.* **10** 2111–6
[22] Naik G V, Shalaev V M and Boltasseva A 2013 *Adv. Mater.* **25** 3264–94
[23] Rizza C, Di Falco A and Ciattoni A 2011 *Appl. Phys. Lett.* **99** 221107
[24] Maas R, Parsons J, Engheta N and Polman A 2013 *Nat. Photon.* **7** 907–12
[25] Pollard R J, Murphy A, Hendren W R, Evans P R, Atkinson R, Wurtz G A, Zayats A V and Podolskiy V A 2009 *Phys. Rev. Lett.* **102** 127405
[26] Yun S, Jiang Z H, Xu Q, Liu Z, Werner D H and Mayer T S 2012 *ACS Nano* **6** 4475–82
[27] Jackson J D 2007 *Classical Electrodynamics* (New York: Wiley)
[28] Born M, Wolf E and Bhatia A B 1999 *Principles of Optics: Electromagnetic Theory of Propagation, Interference and Diffraction of Light* (Cambridge: Cambridge University Press)
[29] Javani M H and Stockman M I 2016 *Phys. Rev. Lett.* **117** 107404
[30] Huang X, Lai Y, Hang Z H, Zheng H and Chan C T 2011 *Nat. Mater.* **10** 582–6
[31] Sakoda K 2012 *Opt. Express* **20** 3898–917
[32] Sakoda K 2012 *J. Opt. Soc. Am.* B **29** 2770–8
[33] Moitra P, Yang Y, Anderson Z, Kravchenko I I, Briggs D P and Valentine J 2013 *Nat. Photon.* **7** 791–5
[34] Li Y, Kita S, Muñoz P, Reshef O, Vulis D I, Yin M, Lončar M and Mazur E 2015 *Nat. Photon.* **9** 738–42
[35] Castro Neto A H, Peres N M R, Novoselov K S and Geim A K 2009 *Rev. Mod. Phys.* **81** 109–62
[36] Kita S, Li Y, Camayd-Muñoz P, Reshef O, Vulis D I, Day R W, Mazur E and Lončar M 2017 *Opt. Express* **25** 8326–34
[37] Vulis D I, Li Y, Reshef O, Camayd-Muñoz P, Yin M, Kita S, Lončar M and Mazur E 2017 *Opt. Express* **25** 12381–99
[38] Collins M J, Zhang F, Bojko R, Chrostowski L and Rechtsman M C 2016 *Phys. Rev.* A **94** 063827
[39] Zhen B, Hsu C W, Igarashi Y, Lu L, Kaminer I, Pick A, Chua S L, Joannopoulos J D and Soljačić M 2015 *Nature* **525** 354–8
[40] Kamiński P M, Taghizadeh A, Breinbjerg O, Mørk J and Arslanagić S 2017 *Opt. Lett.* **42** 2866
[41] Mao Q, Xie K, Hu L, Li Q, Zhang W, Jiang H, Hu Z and Wang E 2016 *Appl. Opt.* **55** 139–43
[42] Luo J, Lu W, Hang Z, Chen H, Hou B, Lai Y and Chan C 2014 *Phys. Rev. Lett.* **112** 073903
[43] Mahmoud A M and Engheta N 2014 *Nat. Commun.* **5** 1–7
[44] Memarian M and Eleftheriades G V 2015 *Nat. Commun.* **6** 5855
[45] Hajian H, Ozbay E and Caglayan H 2016 *Appl. Phys. Lett.* **109** 031105
[46] He X T, Huang Z Z, Chang M L, Xu S Z, Zhao F L, Deng S Z, She J C and Dong J W 2016 *ACS Photonics* **3** 2262–7
[47] Mattiucci N, Bloemer M and D'Aguanno G 2013 *Opt. Express* **21** 11862–8
[48] Mattiucci N, Bloemer M J, Aguanno G D, Facility C M B and Arsenal R 2014 *Opt. Express* **22** 9–17
[49] DAguanno G, Mattiucci N, Conti C and Bloemer M J 2013 *Phys. Rev. B: Condens. Matter* **87** 085135
[50] Alù A, Silveirinha M G and Engheta N 2008 *Phys. Rev.* E **78** 016604
[51] Edwards B, Alù A, Young M E, Silveirinha M and Engheta N 2008 *Phys. Rev. Lett.* **100**
[52] Edwards B, Al A, Silveirinha M G and Engheta N 2009 *J. Appl. Phys.* **105** 044905
[53] Marcos J S, Silveirinha M G and Engheta N 2015 *Phys. Rev. B: Condens. Matter* **91** 195112
[54] Feng Ma H, Hui Shi J, Cheng Q and Jun Cui T 2013 *Appl. Phys. Lett.* **103** 021908
[55] Qiu P, Qiu W, Lin Z, Chen H, Ren J, Wang J X, Kan Q and Pan J Q 2017 *Sci. Rep.* **7** 9588
[56] D'Aguanno G, Centini M, Scalora M, Sibilia C, Bloemer M J, Bowden C M, Haus J W and Bertolotti M 2001 *Phys. Rev.* E **63** 036610
[57] Solli D R, McCormick C F, Chiao R Y and Hickmann J M 2003 *IEEE J. Sel. Top. Quantum Electron.* **9** 40–2
[58] Chiao R Y, Kwiat P G and Steinberg A M 1991 *Phys. B: Condens. Matter* **175** 257–62
[59] Steinberg A M, Kwiat P G and Chiao R Y 1993 *Phys. Rev. Lett.* **71** 708–11

[60] Joannopoulos J D, Johnson S G, Winn J N and Meade R D 2011 *Photonic Crystals: Molding the Flow of Light* 2nd edn (Princeton, NJ: Princeton University Press)
[61] Kocaman S, Aras M S, Hsieh P, McMillan J F, Biris C G, Panoiu N C, Yu M B, Kwong D L, Stein A and Wong C W 2011 *Nat. Photon.* **5** 499–505
[62] Lončar M, Nedeljković D, Pearsall T P, Vučković J, Scherer A, Kuchinsky S and Allan D C 2002 *Appl. Phys. Lett.* **80** 1689–91
[63] Schulz S A, O'Faolain L, Beggs D M, White T P, Melloni A and Krauss T F 2010 *J. Opt.* **12** 104004
[64] Notomi M, Yamada K, Shinya A, Takahashi J, Takahashi C and Yokohama I 2001 *Phys. Rev. Lett.* **87** 253902
[65] Stockman M I 2006 Does nature allow negative refraction with low losses in optical region? arXiv:cond-mat/0611350
[66] Soukoulis C M and Wegener M 2011 *Nat. Photon.* **5** 523–30
[67] Jahani S and Jacob Z 2016 *Nat. Nanotechnol.* **11** 23–36
[68] Zhao Q, Zhou J, Zhang F and Lippens D 2009 *Mater. Today* **12** 60–9
[69] Enkrich C, Wegener M, Linden S, Burger S, Zschiedrich L, Schmidt F, Zhou J F, Koschny T and Soukoulis C M 2005 *Phys. Rev. Lett.* **95** 203901
[70] Dolling G, Enkrich C, Wegener M, Zhou J F, Soukoulis C M and Linden S 2005 *Opt. Lett.* **30** 3198–200
[71] Pendry J B, Holden A J, Robbins D J and Stewart W J 1999 *IEEE Trans. Microw. Theory Tech.* **47** 2075–84
[72] Cai W and Shalaev V 2010 *Optical Metamaterials: Fundamentals and Applications* (New York: Springer) pp 77–100
[73] Smith D R, Padilla W J, Vier D C, Nemat-Nasser S C and Schultz S 2000 *Phys. Rev. Lett.* **84** 4184–7
[74] Huangfu J, Ran L, Chen H, Zhang X M, Chen K, Grzegorczyk T M and Kong J A 2004 *Appl. Phys. Lett.* **84** 1537–9
[75] Shalaev V M, Cai W, Chettiar U K, Yuan H K, Sarychev A K, Drachev V P and Kildishev A V 2005 *Opt. Lett.* **30** 3356–8
[76] Lezec H J, Dionne J A and Atwater H A 2007 *Science* **316** 430–2
[77] Zhang S, Fan W, Panoiu N C, Malloy K J, Osgood R M and Brueck S R J 2005 *Phys. Rev. Lett.* **95** 137404
[78] Dolling G, Enkrich C, Wegener M, Soukoulis C M and Linden S 2006 *Opt. Lett.* **31** 1800–2
[79] Valentine J, Zhang S, Zentgraf T, Ulin-Avila E, Genov D A, Bartal G and Zhang X 2008 *Nature* **455** 376–9
[80] Lewin L 1947 *J. Inst. Electr. Eng.—Part III: Radio Commun. Eng.* **94** 65–8
[81] Bohren C F and Huffman D R 2008 *Absorption and Scattering of Light by Small Particles* (New York: Wiley)
[82] O'Brien S and Pendry J B 2002 *J. Phys.: Condens. Matter* **14** 4035
[83] Holloway C L, Kuester E F, Baker-Jarvis J and Kabos P 2003 *IEEE Trans. Antennas Propag.* **51** 2596–603
[84] Pfeiffer C and Grbic A 2013 *Phys. Rev. Lett.* **110** 197401
[85] Shcherbakov M R, Vabishchevich P P, Shorokhov A S, Chong K E, Choi D Y, Staude I, Miroshnichenko A E, Neshev D N, Fedyanin A A and Kivshar Y S 2015 *Nano Lett.* **15** 6985–90
[86] Liu W 2017 *Phys. Rev. Lett.* **119** 123902
[87] Liu W, Sun Y, Lai Z and Chen H 2017 *J. Opt. Soc. Am.* B **34** 1899–904
[88] Yang Z J, Zhao Q and He J 2017 *Opt. Express* **25** 15927–37
[89] Schuller J A, Zia R, Taubner T and Brongersma M L 2007 *Phys. Rev. Lett.* **99** 725
[90] Vynck K, Felbacq D, Centeno E, Căbuz A I, Cassagne D and Guizal B 2009 *Phys. Rev. Lett.* **102** 133901
[91] Peng L, Ran L, Chen H, Zhang H, Kong J A and Grzegorczyk T M 2007 *Phys. Rev. Lett.* **98** 157403
[92] Wu Y, Li J, Zhang Z Q and Chan C T 2006 *Phys. Rev. B: Condens. Matter* **74** 085111
[93] Smith D R, Vier D C, Koschny T and Soukoulis C M 2005 *Phys. Rev.* E **71** 1–11
[94] Notomi M 2000 *Phys. Rev. B: Condens. Matter* **62** 10696–705
[95] Brown J 1953 *Proc. IEE—Part IV: Inst. Monogr.* 100 51–62
[96] Sakoda K 2012 *Opt. Express* **20** 25181–94
[97] Foteinopoulou S 2012 *Phys. B: Condens. Matter* **407** 4056–61
[98] Li Y, Wu Y, Chen X and Mei J 2013 *Opt. Express* **21** 7699–711
[99] Faryad M and Ashraf M W 2016 *J. Opt. Soc. Am.* B **33** 1008–13
[100] Dubois M, Shi C, Zhu X, Wang Y and Zhang X 2017 *Nat. Commun.* **8** 14871
[101] Li Y, Camayd-Muñoz P, Vulis D, Saeta P, Peng Y, Reshef O, Mello O L, Tang H, Lončar M and Mazur E 2017 Transition metamaterials for local-field enhancement *Conf. on Lasers and Electro-Optics* (Optical Society of America) p FM3G.6
[102] Popovic M A, Barwicz T, Ippen E P and Kartner F X 2006 Conference on Lasers and Electro-Optics 2006 *IEEE Quantum Electronics and Laser Science Conference* pp 1–2
[103] Djordjevic S S, Shang K, Guan B, Cheung S T S, Liao L, Basak J, Liu H F and Yoo S J B 2013 *Opt. Express* **21** 13958–68
[104] Mirzaei A, Shadrivov I V, Miroshnichenko A E and Kivshar Y S 2013 *Opt. Express* **21** 10454–9
[105] Paniagua-Dominguez R, Lopez-Tejeira F, Marques R and Sanchez-Gil J A 2011 *New J. Phys.* **13** 123017
[106] Li Y and Mei J 2015 *Opt. Express* **23** 12089–99
[107] Li Y, Wu Y and Mei J 2014 *Appl. Phys. Lett.* **105** 014107
[108] Ashraf M W and Faryad M 2015 *J. Opt. Soc. Am.* B **9** 093057
[109] Wang J R, Chen X D, Zhao F L and Dong J W 2016 *Sci. Rep.* **6** 22739
[110] Lapine M, Shadrivov I V, Powell D A and Kivshar Y S 2011 *Nat. Mater.* **11** 30–3
[111] van de Groep J and Polman A 2013 *Opt. Express* **21** 26285
[112] Xu D X, Schmid J H, Reed G T, Mashanovich G Z, Thomson D J, Nedeljkovic M, Chen X, Van Thourhout D, Keyvaninia S and Selvaraja S K 2014 *IEEE J. Sel. Top. Quantum Electron.* **20** 189–205
[113] Yariv A 1997 *Optical Electronics in Modern Communications* (Oxford: Oxford University Press)
[114] Lin Z, Christakis L, Li Y, Mazur E, Rodriguez A W and Lončar M 2018 *Phys. Rev. B: Condens. Matter* **97** 081408
[115] Makris K G, El-Ganainy R, Christodoulides D N and Musslimani Z H 2008 *Phys. Rev. Lett.* **100** 103904
[116] Szameit A, Rechtsman M C, Bahat-Treidel O and Segev M 2011 *Phys. Rev.* A **84** 021806
[117] Nagai S and Sanada A 2016 *IEICE Electron. Express* **13**
[118] Davanco M, Urzhumov Y and Shvets G 2007 *Opt. Express* **15** 9681–91
[119] Fietz C, Urzhumov Y and Shvets G 2011 *Opt. Express* **19** 19027–41
[120] Reshef O, Camayd-Mu noz P, Vulis D I, Li Y, Lončar M, Mazur E, Lončar M and Mazur E 2017 *ACS Photonics* **4** 2385–9
[121] Gao H, Zhou Y S, Zheng Z Y, Chen S J and Dong J J 2017 *Appl. Phys.* B **123** 165
[122] Simovski C R and Tretyakov S A 2007 *Phys. Rev. B: Condens. Matter* **75** 195111
[123] Hsu C W, Zhen B, Douglas Stone A, Joannopoulos J D and Soljačić M 2016 *Nat. Rev. Mater.* **1** 16048
[124] Muñoz P, Kita S, Mello O, Reshef O, Vulis D I, Li Y, Loncar M and Mazur E 2016 Lossless integrated Dirac-cone metamaterials *Conf. on Lasers and Electro-Optics* (Optical Society of America) p JW2A.24v

Daryl I Vulis received her PhD in Applied Physics from Harvard University where she specialized in metamaterials and integrated photonics. She is the recipient of both the National Defense Science & Engineering Graduate Fellowship and the National Science Foundation Graduate Fellowship, and she has held research positions at Cornell University, the University of Geneva, and the National Institute for Materials Science in Japan. She currently works at Apple Inc. in Cupertino, California.

Orad Reshef is a Canadian applied physicist working in nanophotonics, metamaterials and nonlinear optics. He is interested in scalable integrated photonic devices, and in engineering nonlinear interactions and devices that are not typically found in nature by structuring materials on the nanoscale. He received his PhD from Harvard University in 2016, and is currently a Banting postdoctoral fellow at the CERC group in the University of Ottawa.

Eric Mazur is an experimental physicist specializing in light matter interactions and nanophotonics. He obtained his PhD from the University of Leiden and then moved to the US to accept a postdoctoral position at Harvard University. After a brief postdoc, he joined the faculty, where he remains to this day. Mazur was the 2017 President of the Optical Society and holds honorary doctorates from the Ecole Polytechnique in Montreal and the Universidad Nacional Mayor de San Marcos in Lima, as well as a number of honorary professorship in China.